Available online at www.sciencedirect.com
ScienceDirect
Journal of Sound and Vibration 313 (2008) 97–112
JOURNAL OF SOUND AND VIBRATION
www.elsevier.com/locate/jsvi

A method for quantifying the acoustic transfer function of a ducted rotor

D.B. Stephens*, S.C. Morris

Hessert Research Laboratory, University of Notre Dame, Notre Dame, IN 46556, USA

Received 11 February 2006; received in revised form 4 June 2007; accepted 19 June 2007
Available online 22 January 2008

Abstract

This paper describes a method for analyzing the sound radiated by a low-speed axial flow ducted fan. The radiated sound depends on both the sound generated by the rotor and the geometry of the surfaces surrounding the source region. These surfaces act to modify the spectral content of the sound as perceived by an observer outside of the duct. The fan was considered as a compact region of axial dipole sources, so that the radiated sound could be described as the product of a frequency-dependent unsteady force and an effective transfer function. The primary goal of this study was to develop a method for quantifying the acoustic transfer function for this general class of system using radiated sound measurements. Microphone measurements were acquired of the radiated sound generated by a ten-bladed fan operating inside a finite length rigid duct. Two fundamental frequencies were found to be inherent in the system, one based on the parameters of the sound source, and the other based on the geometry of the duct. As previous studies have found, these two frequency scales allow for the separation of the radiated sound into source and transfer function spectra. A unique method for determining these separate functions is presented, with the primary assumption that the aeroacoustic sources follow a power law relationship with rotor tip relative speed. The resulting algorithm was shown to effectively quantify the acoustic transfer function. A set of mathematically defined input functions was used to evaluate the efficacy of the separation method. Additionally, the ducted rotor system was operated over a range of flow rates to produce different sound sources, and the transfer function calculated by the algorithm was found to be independent of this source mechanism.

1. Introduction

Axial flow ducted rotors are important in numerous engineering applications, ranging from ventilation equipment to jet engines. The aerodynamic sound radiated from these devices is generated by a number of different mechanisms. At low speeds these mechanisms can be generally described by the response of the rotor to turbulent flows. For example, the interaction between the blades and turbulence in the approach flow is often referred to as "inflow noise." Sound generated by the scattering of unsteady pressure that is created by the blades is often referred to as "self noise." Many of these sound sources have received extensive analytical attention, much of which can be found in books by Blake [1] and Goldstein [2], and review papers by Morfey [3],

*Corresponding author.
E-mail addresses: Stephens.25@nd.edu (D.B. Stephens), S.Morris@nd.edu (S.C. Morris).

0022-460X/$ - see front matter © 2007 Elsevier Ltd. All rights reserved.
doi:10.1016/j.jsv.2007.11.054

Nomenclature

B	number of rotor blades
BPF	blade passing frequency, ($B\Omega$)
c_0	speed of sound
D	duct diameter
D_r	rotor diameter
f	frequency
$\mathbf{F}$	body force distribution leading to dipole sound
$\mathscr{F}$	net sound source spectral function
g	Green's function defined by Eq. (4)
g_{fs}	Green's function for a point source in an unbounded fluid at rest
He	Helmholtz number, (fD/c_0)
k	acoustic wavenumber, ($2\pi f/c_0$)
M_{tip}	Mach number based on rotor tip speed, (U_{tip}/c_0)
$n(St)$	sound source tip speed exponent
p	Fourier transform of unsteady pressure
p_{ref}	reference pressure, 20 mPa
$\mathscr{P}$	autospectrum of p
$\mathbf{r}$	far-field observer location
$\mathbf{r}_0$	sound source location
SR	speed ratio, ($\Omega_{\max}/\Omega_{\min}$)
St	strouhal number, ($fD_r\pi/V_{\mathrm{tip}}B = f/\mathrm{BPF}$)
$\mathscr{T}$	net acoustic transfer function, Eq. (16)
U_0	spatial mean axial velocity inside duct
V_0	volume of distributed acoustic sources
V_{tip}	rotor tip velocity, ($\Omega D_r/2$)
U_{tip}	relative fluid velocity at rotor tip, ($\sqrt{(1+\phi^2)}V_{\mathrm{tip}}$)
θ	angle between axis of dipole and $\mathbf{r}-\mathbf{r}_0$
ϕ	flow coefficient, (U_0/U_{tip})
χ	amplification factor of transfer function due to duct
Ω	rotor rotation frequency, ($V_{\mathrm{tip}}/\pi D_r$)

Wright [4] and Huff [5]. Some examples of more recent work include rotor interactions with the duct boundary layer [6], tip vortex noise [7], trailing vortex sheet noise [8] and ingested flow irregularities [9,10].

The propagation of acoustic waves from rotating sources can be represented by an appropriate Green's function. Sound propagation from rotors operating in a free-space environment can be found by using a free-space Green's function with modifications for rotational effects (see, e.g., Ref. [1]). Rotors operating in an effectively infinite duct invoke significantly more complex phenomena due to the effects of the source distribution on the excitation of various duct characteristic modes (see e.g. [11–13]). Noise that is radiated from rotors operating in a relatively short duct section exhibits additional complexity. For example, reflected waves from the duct ends will result in "organ-pipe" modes whose amplitude will depend on the location of the sources. The directivity and amplitude of sound radiated from each of the duct ends depends on the specific geometry of the duct inlet and exit sections. The Green's function for a finite length duct cannot be determined analytically, and so must be measured or computed numerically. For example, boundary element methods (BEM) are effective, but require significant computational resources, particularly for very complex geometries.

The relationship between the generated sound and the far-field sound propagation can be simplified significantly by considering the sound source to be a net equivalent dipole force, $\mathscr{F}(St, M_{\mathrm{tip}})$. The tip relative Mach number M_{tip} is defined as the relative fluid velocity at the tip, U_{tip}, divided by the speed of sound in the working fluid, c_0. The independent frequency variable is described as a Strouhal number, in the manner of Weidemann [14], and defined as

$$St = \frac{fD_r\pi}{V_{\mathrm{tip}}B} = \frac{f2\pi}{\Omega B} = \frac{f}{\mathrm{BPF}}, \tag{1}$$

where D_r is the rotor diameter, V_{tip} is the velocity of the rotor tip, f is the dimensional frequency and B is the number of rotor blades. For this definition the fundamental frequency of the sound source is taken to be the rotor blade passing frequency (BPF). The effects of the Green's function can be considered as a net transfer function, $\mathscr{T}(He)$, where the Helmholtz number is defined as

$$He = \frac{fD}{c_0} = M_{\mathrm{tip}} \times St \times \frac{B}{\pi}, \tag{2}$$

where D is the duct diameter.

The sound spectrum at a point in the far field is then given by the product, $\mathscr{P} = \mathscr{F} \cdot \mathscr{T}$. A complete derivation of this relationship and its assumptions is given in the following section. The focus of the present investigation is the use of experimental measurements of the radiated sound spectra, $\mathscr{P}(f, M_{\text{tip}})$, to quantify the two functions $\mathscr{F}(St, M_{\text{tip}})$ and $\mathscr{T}(He)$. These measurements utilized a low-speed fan operated inside of a short annular duct section inside an anechoic room. The radiated sound spectra were acquired using a single far-field microphone at 11 rotational speeds.

A number of previous investigations have explored methods for separating source and transfer effects from measurements of the radiated sound [14–18]. A thorough discussion of these and other related papers will be given in the following section, along with the relevant background material. A new code was written for each of these methods and applied to the present data set. All of these methods were found to identify the majority of the spectral features in both $\mathscr{F}$ and $\mathscr{T}$. However, in each case the results were found to exhibit spurious trends in both $\mathscr{T}$ and $\mathscr{F}$. Specifically, these methods were found to result in functions for $\mathscr{T}$ that were strongly dependent on the spectral content of the sound source. It will be shown in this paper that these errors are likely due to a non-uniqueness issue that has not previously been described and accounted for. Specifically, it will be shown that large-scale trends in either $\mathscr{F}$ or $\mathscr{T}$ cannot be determined by simply varying the fan speed.

The main result of this paper is the presentation of a new formulation and algorithm for determining $\mathscr{F}$ and $\mathscr{T}$ from the available measurements. The background and assumptions are provided in the following section. The efficacy of the algorithm was tested using a new experimental database as well as mathematically defined input functions. The experiments included measurements with dramatically varied acoustic source spectra that resulted from throttling the fan into rotating stall. The functions $\mathscr{T}$ returned from these tests varied by less than 0.29 dB across most of the frequency range of interest.

2. Analytical background

2.1. Derivation of net equivalent product model

A system that can be characterized as a compact distribution of aeroacoustic sources surrounded by a specified geometry gives rise to the conceptual framework of a net equivalent point source and an effective acoustic transfer function. This concept can be formalized by starting with the Helmholtz equation,

$$\nabla^2 p + k^2 p = \nabla \cdot \mathbf{F}, \tag{3}$$

where p is the Fourier transform of the acoustic pressure and k is the acoustic wavenumber. The form of the acoustic source on the right-hand side is assumed to be dipole in nature where $\mathbf{F}$ is an equivalent body force distribution. Eq. (3) is valid for low Mach number systems without monopole or quadrupole type sources.

The Helmholtz equation can be solved using a Green's function approach, where Green's function $g(\mathbf{r}, \mathbf{r}_0)$ is explicitly defined by

$$\nabla^2 g(\mathbf{r}, \mathbf{r}_0) + k^2 g(\mathbf{r}, \mathbf{r}_0) = -\delta(\mathbf{r} - \mathbf{r}_0) \tag{4}$$

and the boundary conditions appropriate to the system. For Eq. (4), $\mathbf{r}_0$ is the source location, $\mathbf{r}$ is the observer location, and δ is the Kronecker delta function. The solution to Eq. (3) can be written as a convolution of the Green's function over a volume V_0 with the distributed sources $\nabla \cdot \mathbf{F}$, giving

$$p(\mathbf{r}) = \iiint_V [-\nabla_0 \cdot \mathbf{F}] g(\mathbf{r}, \mathbf{r}_0)\, \mathrm{d}V_0, \tag{5}$$

where the subscript on the operator ∇_0 denotes operation over the source region. A detailed derivation of Eq. (5) is available in Ref. [19], among others. Integration by parts allows the far-field solution to be rewritten as

$$p(\mathbf{r}) = \iiint_V \mathbf{F} \cdot \nabla_0 g(\mathbf{r}, \mathbf{r}_0)\, \mathrm{d}V_0. \tag{6}$$

If the source region is sufficiently compact the Green's function is separable into near and far-field components. By using a coordinate system centered about the source region, this assumption of compactness

is denoted as $k|\mathbf{r}_0| \ll 1$. For the purposes of this paper, it will be useful to describe the Green's function as a product of three functions,

$$g(\mathbf{r}, \mathbf{r}_0) = \chi(\mathbf{r}) g_{\text{fs}}(\mathbf{r}, \mathbf{r}_0) g_{\text{near}}(\mathbf{r}_0), \tag{7}$$

where g_{near} is a dimensionless function of the source location that quantifies near-field effects such as Doppler shifts due to moving sources, geometrical non-compactness, and other effects due to both propagating and non-propagating components. The dimensions of the Green's function are retained in the free-space Green's function, $g_{\text{fs}} = (1/4\pi|\mathbf{r} - \mathbf{r}_0|)\mathrm{e}^{\mathrm{i}k|\mathbf{r}-\mathbf{r}_0|}$. The function χ accounts for amplifications and attenuations at particular frequencies due to the boundary conditions imposed by the rigid duct. A similar amplification function was introduced by Morse and Ingard [19, p. 320]. As an example, if a harmonic monopole source were placed near an infinite rigid wall, the magnitude amplification function would be $|\chi| = 2$, indicating a doubling of the magnitude of the free space Green's function across all frequencies.

Combining Eq. (7) with Eq. (6) gives

$$p(\mathbf{r}) = \chi(\mathbf{r}) \iiint_V \mathbf{F} \cdot \nabla_0 [g_{\text{fs}}(\mathbf{r}, \mathbf{r}_0) g_{\text{near}}(\mathbf{r}_0)] \, \mathrm{d}V_0. \tag{8}$$

For the ducted rotor system considered in this paper, a radiation efficiency term can be partially derived by considering the acoustic sources to be axially oriented dipoles. This is appropriate so long as the stagger of the blades is such that the unsteady forcing on the rotor blades acts primarily in the axial direction. An equivalent source distribution can be defined as

$$\mathbf{F}(\mathbf{r}_0) = F_x(\mathbf{r}_0), \tag{9}$$

where the unsteady forces act only in the x-direction, that is along the axis of the duct, denoted with the subscript x. The gradient operator in Eq. (8) can be carried out giving

$$p(\mathbf{r}) = \chi(\mathbf{r}) \iiint_V F_x [\nabla_0 g_{\text{fs}}(\mathbf{r}, \mathbf{r}_0) g_{\text{near}} + g_{\text{fs}}(\mathbf{r}, \mathbf{r}_0) \nabla_0 g_{\text{near}}(\mathbf{r}_0)] \, \mathrm{d}V_0. \tag{10}$$

The gradient of the free space Green's function in the far field is given as

$$\nabla_0 g_{\text{fs}}(\mathbf{r}, \mathbf{r}_0) = -[\mathrm{i}k \cos\theta] g_{\text{fs}}(\mathbf{r}, \mathbf{r}_0), \tag{11}$$

where θ is the angle between the axis of the dipole forces and the vector between the source and the receiver, $\mathbf{r} - \mathbf{r}_0$. Substituting this in Eq. (10) gives

$$p(\mathbf{r}) = \chi(\mathbf{r}) \iiint_V F_x (\mathrm{i}k) g_{\text{fs}}(\mathbf{r}, \mathbf{r}_0) \cos\theta \left[g_{\text{near}} + \frac{\nabla_0 g_{\text{near}}(\mathbf{r}_0)}{\mathrm{i}k \cos\theta} \right] \mathrm{d}V_0. \tag{12}$$

If $|\mathbf{r} - \mathbf{r}_0|$ can be approximated as $|\mathbf{r}|$, then g_{fs} can be removed from the integral above, which is appropriate now that the gradient operator has been evaluated and the dependence of g_{fs} on $\mathbf{r}_0$ is small. This gives

$$p(\mathbf{r}) = -\chi(\mathbf{r})(\mathrm{i}k) g_{\text{fs}}(\mathbf{r}) \cos\theta \iiint_V F_x \left[g_{\text{near}}(\mathbf{r}_0) + \frac{\nabla_0 g_{\text{near}}(\mathbf{r}_0)}{\mathrm{i}k \cos\theta} \right] \mathrm{d}V_0. \tag{13}$$

The autospectrum of the acoustic pressure can be obtained by taking the expected value of Eq. (13) multiplied by its complex conjugate to obtain

$$\begin{aligned} \mathscr{P} = \overline{p^2}(\mathbf{r}) = |\chi(\mathbf{r})|^2 k^2 |g_{\text{fs}}(\mathbf{r})|^2 \cos^2\theta \iiint_{V_2} \cdot \iiint_{V_1} \overline{F_{i1} F_{i2}^*} \\ \times \left[g_{\text{near}}(\mathbf{r}_{01}) + \frac{\nabla_{01} g_{\text{near}}(\mathbf{r}_{01})}{\mathrm{i}k \cos\theta} \right] \left[g_{\text{near}}(\mathbf{r}_{02}) + \frac{\nabla_{02} g_{\text{near}}(\mathbf{r}_{02})}{\mathrm{i}k \cos\theta} \right]^* \mathrm{d}V_{01} \, \mathrm{d}V_{02}. \end{aligned} \tag{14}$$

Similar forms of this expression have been derived previously by Blake [1] and Zhang et al. [18], among others. The derivation presented here is unique, however, due to the inclusion of the k^2 efficiency term and the function χ. The net equivalent product model can now be given by representing the spatial integral of the two

point correlation of the distributed sources as a single source function $\mathscr{F}$, yielding

$$\mathscr{P} = \mathscr{F} \cdot \mathscr{T}. \tag{15}$$

The use of the notation $\mathscr{T}$ for the acoustic transfer function is unique to the present communication, and is used to denote the combined variables

$$\mathscr{T} = |\chi(\mathbf{r})|^2 k^2 |g_{\mathrm{fs}}(\mathbf{r})|^2 \cos^2\theta \tag{16}$$

or

$$\log \mathscr{T} = \log k^2 + \log |g_{\mathrm{fs}}|^2 + \log |\chi|^2 + \log \cos^2\theta. \tag{17}$$

which is valid for a compact distribution of axial dipoles.

2.2. Separation of source and transfer functions

The utility of the linear source-filter model given by Eq. (15) is apparent both for analysis of experimental data and for the prediction of acoustic signatures from complex systems. A partial separation of $\mathscr{F}$ from $\mathscr{T}$ given a set of acoustic measurements $\mathscr{P}$ is possible because the acoustic sources are explicitly dependent on a frequency related to the fluid velocity, whereas the transfer function is related only to the geometry of the surrounding surfaces and the sound speed in the working fluid. Eq. (15) can be given as

$$\log \mathscr{P}(f) = \log \mathscr{F}(St) + \log \mathscr{T}(He), \tag{18}$$

where it is now clear that Eq. (14) has been reduced to two terms and that $\mathscr{F}$ is dependent on St but not on He, while $\mathscr{T}$ is dependent on He but not on St.

Before considering specific methodologies for separating the source and transfer functions, it will be useful to develop some insight into the limitations of the analysis. Consider a velocity-dependent source function, $\mathscr{F}(St)$, which is broadband in nature, and a transfer function with a single, narrow band tone at a fixed frequency. An "organ-pipe" type of resonance, for example, could result in such a feature. As the fan speed increases, the radiated sound pressure would likely increase with rotational speed according to a power law. However, each of these measured spectra would exhibit the spectral feature due to the pipe resonance at the fixed frequency. Separating this feature of the acoustic transfer function from the source function is relatively straightforward in this case. In the converse of this example, consider a featureless transfer function, such as the free-space Green's function, and a source spectra with a narrow band feature, such as a blade rate tone. In this case, varying the fan speed will result in radiated sound spectra in which the frequency of the narrow band feature is proportional to the rotor speed. Separating the features of these functions is again straightforward.

It is clear from Eq. (18), however, that absolute magnitudes of $\mathscr{F}$ and $\mathscr{T}$ cannot be uniquely determined using only measurements of $\mathscr{P}$. What is less obvious, is that broad trends cannot be determined by making finite variations in St or He. For a simple example, assume a measured sound spectra which is constant with frequency. Such a spectra could be generated by a source spectra that increases with frequency combined with a transfer function that decreases with frequency, or vice versa. Thus, an important aspect of any algorithm designed to separate $\mathscr{F}$ from $\mathscr{T}$ must delineate which features of the acoustic transfer function can be determined unambiguously, and which features and trends cannot be determined.

Previous attempts at separating the acoustic transfer function from the acoustic sources are described by Weidemann [14] and Neise [15] for centrifugal rotors. A study by Neise and Barsikow [20] used a series of dimensionally similar centrifugal fans to study acoustic similarity laws and reported that the acoustic transfer function spectra were strongly dependent on the rotor flow coefficient ϕ, defined as the mean flow velocity in the duct normalized by rotor tip velocity. In terms of Eq. (18), the term $\mathscr{F}$ should be dependent on the flow coefficient, but the acoustic transfer function $\mathscr{T}$ should not be. In the present derivation, changes in the radiation efficiency with flow coefficient are contained in the near-field term g_{near}, which is contained in $\mathscr{F}$. The finding of Neise and Barsikow may have been a result of the underdetermined aspect of the formulation and their separation method. The results presented in the current work suggest that the acoustic transfer function $\mathscr{T}$ is not a function of rotor flow coefficient.

Mongeau et al. [17] developed a method for characterizing the transfer function for a ducted centrifugal compressor. A similar technique was later applied to a confined jet flow by Zhang et al. [18]. Their method requires the assumption that on a plot of non-dimensional sound pressure spectra in terms of St, lines of constant He are parallel, with an offset determined by the derivative of the transfer function with respect to He. This assumption is valid so long as the acoustic source function $\mathscr{F}(St)$ has only linear variations with St. For example, if one line of He overlaps a blade rate tone, and another He does not, the two lines would not be parallel. These algorithms were found to be effective at determining the small-scale features of the spectral functions. However, application of the method presented by Zhang et al. [18] to the current measurements led to large-scale trends in the acoustic transfer function that were strongly dependent on the functional form of the acoustic sources.

The present technique was developed such that the small-scale features of $\mathscr{T}$ could be determined unambiguously, and the large-scale trends could be intentionally fixed by utilizing additional information known about the acoustic system. The method assumes a function $\mathscr{F}_0$ exists, such that the source spectra at all rotor speeds is given by

$$\mathscr{F}(St, M_{\text{tip}}) = \mathscr{F}_0(St) M_{\text{tip}}^{n(St)}, \tag{19}$$

or

$$\log \mathscr{F}(St, M_{\text{tip}}) = \log \mathscr{F}_0(St) + n(St) \log M_{\text{tip}}. \tag{20}$$

In words, increasing tip speed will result in a linear increase in the logarithm of generated sound pressure at a fixed value of St. The purpose for leaving n as a function of St in Eq. (19) was two fold. First, n can be found as a function of St by a least squares fit to $\mathscr{F}$ and M_{tip} using Eq. (20). Thus leaving n as a function of St seemed to provide the least restrictive assumptions. Second, the tip speed scaling $P \propto V^n$ is given significant attention in the literature, and many different values for tonal and broadband sound have been documented; see, for example, Ref. [15]. The methods developed by Mongeau et al. [17] and Zhang et al. [18] require a fixed value of n but provide results that are explicitly independent of the value of n chosen. A study by Quinlan and Krane [21] reported on the spectral form of the tip speed exponent n, noting that the velocity exponent should be a function of St, but they approximated it as $n(f)$ by using a small change in rotor tip speeds ($\Omega_{\max}/\Omega_{\min} = 1.16$) such that the 'smearing' of spectral features such as blade rate tones over St was minimized. No such approximation will be required of the current work. A detailed study of the resulting function $n(St)$ is beyond the scope of this paper, however.

The main point of this paper is to describe a method for using Eqs. (17), (18) and (20) to find the function χ. The method works by assuming that $P \not\propto V^n$ is due to $\log \chi \neq 0$. That is, radiated sound at the fixed value of St should follow a V^n power law. Deviations from this are assumed to be a result of amplifications and attenuations at specific frequencies He, quantified as the function $\chi(He)$. An algorithm to find the function χ is given in Section 4, and the complete acoustic transfer function $\mathscr{T}$ can be reconstructed using Eq. (17).

3. Ducted rotor experiment

An experimental model of a ducted rotor was constructed in an anechoic chamber, as illustrated in Fig. 1. The model was designed such that the fluid and acoustic boundary conditions could be manipulated and quantified. The duct was constructed from PVC with a machined inner diameter of 206 mm and a wall thickness of 6.7 mm, and supported by a vibration isolation pad. A center cylinder extended upstream of the duct inlet and downstream of the outlet to create an annular flow passage. The inlet flow was conditioned using a single layer of a "cheesecloth" type thin fabric with negligible acoustic impedance stretched over a cylindrical wire frame. A compact servo motor was housed in the center cylinder to direct drive the rotor at the desired speed. The upstream cylinder and motor were supported by eight streamlined struts. The downstream center cylinder was cantilevered from a support structure beyond the duct outlet (not shown). The rotor was a ten-bladed propeller previously used by Sevik [22], with diameter $D = 0.203$ m, constant blade chord $C = 0.025$ m and maximum thickness of 2.4 mm, with straight blades incorporating twist only. The rotor

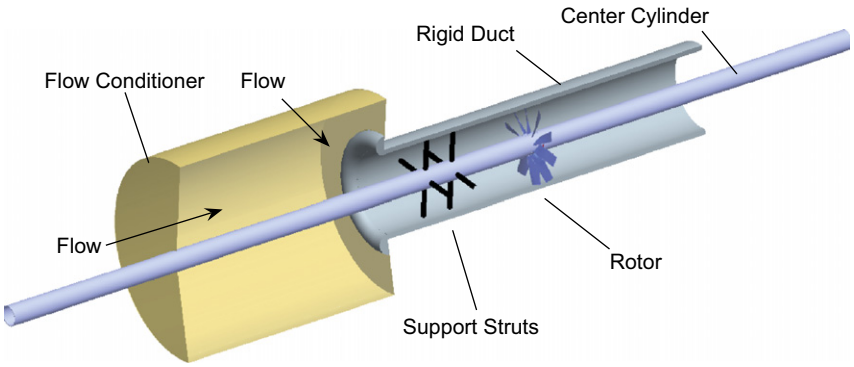

Fig. 1. Schematic of experimental model.

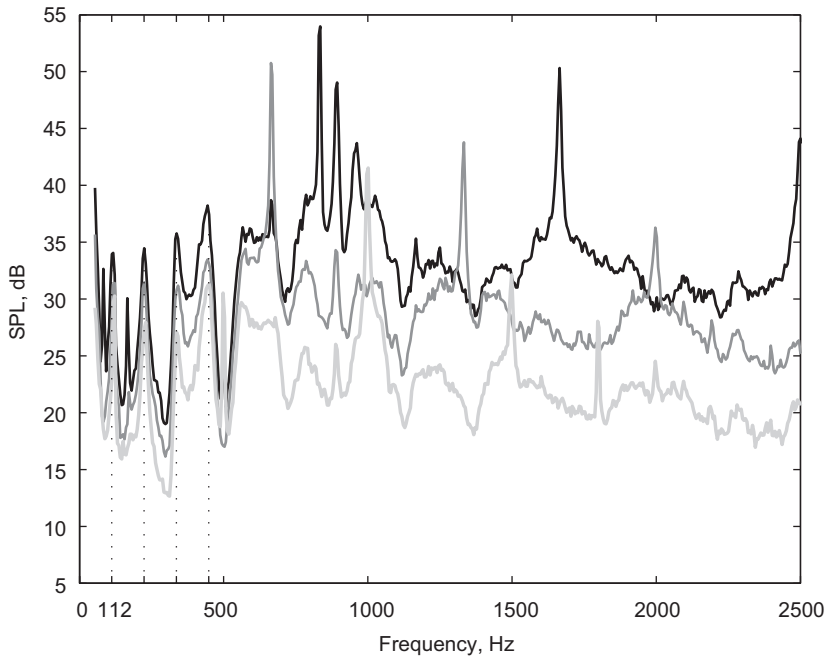

Fig. 2. Measured sound spectra for ducted rotor at three rotational speeds, referenced to p_{ref}. Organ pipe modes can be seen at multiples of 112 Hz. '■': 5000 rev/min; '■': 4000 rev/min; '■': 3000 rev/min.

operated with a tip gap equal to 5% of the blade chord. The length of the duct was 1.4 m and the rotor was positioned 0.56 m from the duct inlet.

Radiated sound was measured using Brüel & Kjær 6.35 mm capacitance based microphones. The microphones were positioned approximately two meters from the duct inlet at an angle of 9.5° from the duct axis. Measurements were acquired at 11 equally spaced speeds from 2500 to 5000 rev/min. Example sound spectra are shown in Figs. 2 and 3. A number of distinctive features were observed in the spectra. For example, multiple "organ pipe" type resonances can be observed at fixed frequencies in Fig. 2. The spectra are plotted as functions of St in Fig. 3 and show distinct features at integer multiples of St, such as blade rate tones. Significant broadband sound was also observed at high frequencies.

The radiated sound was found to be dependent on the rotor flow coefficient ϕ. The duct flow rate was decreased by applying variable restriction in the form of thin fabric with negligible effect on the acoustic field to the duct exit, and increased by attaching the outlet of the duct to the anechoic wind tunnel blower.

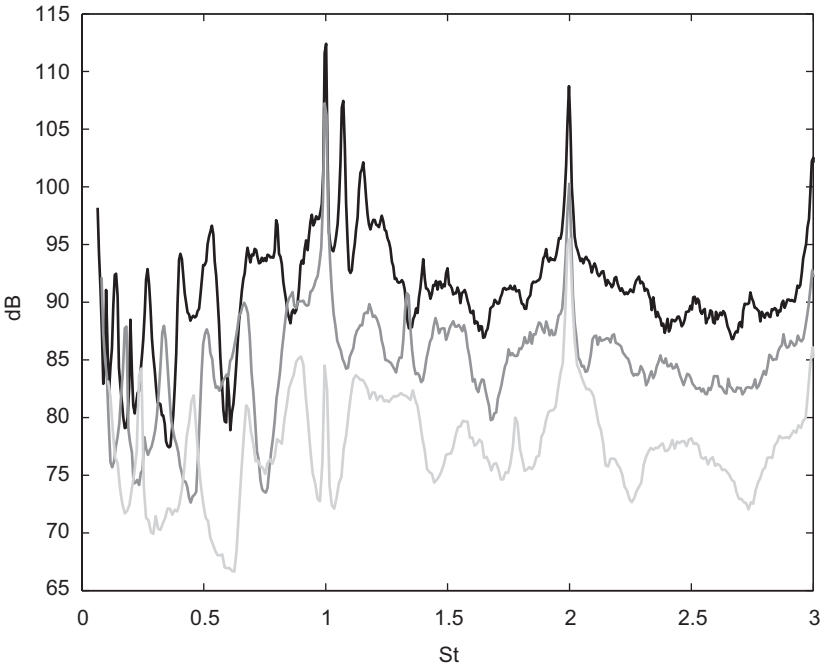

Fig. 3. Measured sound spectra for ducted rotor at three rotational speeds, frequency normalized at St, referenced to p_{ref}. Blade rate tones are readily apparent at integer values of St. '■': 5000 rev/,om; '■': 4000 rev/min; '■': 3000 rev/min.

4. Spectral decomposition algorithm

This section describes an algorithm for using the equations derived in Section 2 to extract an acoustic transfer function spectrum from a series of microphone measurements acquired at a range of rotor tip speeds. The linear model given in Eq. (18) can be expanded by substituting Eq. (20) for $\log \mathscr{F}$ and Eq. (17) for $\log \mathscr{T}$ to obtain

$$\log \mathscr{P}(f, M_{\mathrm{tip}}) = \log \mathscr{F}_0(St) + n(St) \log M_{\mathrm{tip}} + \log k^2 + \log |g_{\mathrm{fs}}|^2 + \log |\chi(He)|^2 + \log \cos^2 \theta. \tag{21}$$

In this expression $\mathscr{F}_0(St)$, $n(St)$ and $\chi(He)$ are unknown. The algorithm seeks to find the function $\chi(He)$ that, in a least squares sense, best fits this expression given measurements of $\mathscr{P}$ at several values of M_{tip}. Once the function $\chi(He)$ has been found, the value of the true acoustic transfer function can then be reconstructed using Eq. (17). The relationship between the source function, the transfer function, and the radiated sound is given in Eq. (18).

4.1. Implementation as a computer algorithm

The method was implemented as an algorithm using Matlab on a desktop computer. Processing time ranged from less than a minute to several minutes, depending primarily on the number of points in the frequency spectra. A flowchart representation of the algorithm is included in Fig. 4 for reference. The algorithm is iterative, and the index j is used in this section to denote terms that are calculated with each iteration.

Step 1: The source spectra for each rotor speed are estimated as

$$\log \mathscr{F}_j(f, M_{\mathrm{tip}}) = \log \mathscr{P}(f, M_{\mathrm{tip}}) - \log k^2 - \log |g_{\mathrm{fs}}|^2 - \log |\chi_j(He)|^2 - \log \cos^2 \theta. \tag{22}$$

For the first iteration ($j = 1$) the function $\log |\chi_{j=1}(He)|^2$ is set equal to zero, and the rest of the terms on the right-hand side of Eq. (22) are known. The impact of this initial value for χ will be discussed in Section 4.2. The spectra are made non-dimensional using the source length πD_r and velocity $V_{\mathrm{tip}}B$ as

$$\mathscr{F}_j(St, M_{\mathrm{tip}}) \equiv (V_{\mathrm{tip}}B/\pi D_r)\mathscr{F}_j(f, M_{\mathrm{tip}}). \tag{23}$$

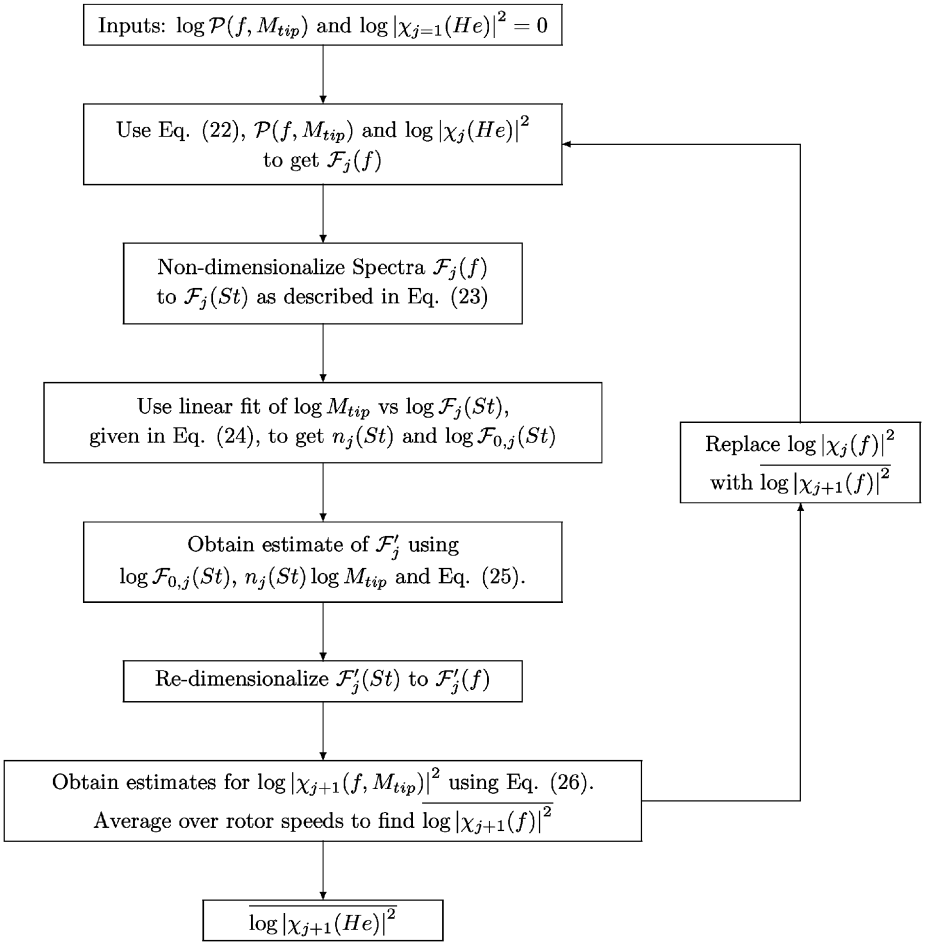

Fig. 4. Flowchart representation of decomposition method. The number of the iteration is denoted by the index j.

This type of spectral scaling is described by Blake [1, p. 38]. Linear interpolation was used to obtain the spectral magnitudes at discrete values of St from $\mathscr{F}_j(f, M_{\text{tip}})$. It was also important to restrict the calculations to the extent of the available data. Specifically, the highest frequency useable was determined by the highest St of the highest speed. As an example, the maximum measured sound frequency of 20 kHz corresponded to $St = 48$ at 2500 rev/min, and $St = 24$ at 5000 rev/min, so the highest St that could be used was 24. The limit of the estimates for $\mathscr{F}_j(St = 24)$ likewise correspond to frequencies of 10–20 kHz, so the lower value of 10 kHz must be used in re-dimensionalizing the functions back to frequency in Step 4 below. The lower limit of the useable range was determined by the useable frequency range of the anechoic facility. A minimum useful frequency of 100 Hz for the present measurements corresponded to $St = 0.24$ for 2500 rev/min and $St = 0.12$ for 5000 rev/min. The limiting usable value of $St = 0.24$ was used, which corresponded to 100 Hz at 2500 rev/min and 200 Hz at 5000 rev/min. The frequency range of usable data is reduced at both ends by the scaling.

Step 2: A least-squares fit to the estimated sound source spectra is used to obtain $n_j(St)$ and $\mathscr{F}_{0,j}(St)$, using the expression provided in Eq. (20), and denoted here with iteration index j as

$$\log \mathscr{F}_j(f, M_{\text{tip}}) = \log \mathscr{F}_{0,j}(St) + n_j(St) \log M_{\text{tip}}. \tag{24}$$

According to this expression, at each value of St, a plot of $\log \mathscr{F}_j(St, M_{\text{tip}})$ vs. $\log M_{\text{tip}}$ should be a straight line with slope $n_j(St)$. Deviations from the linear scaling are assumed to be a result of $\chi \neq \chi_j$, or for the first iteration, $\chi \neq 0$. An example from the ducted rotor experiment is shown in Fig. 5 at $St = 1.02$. In the current

experiment, $\mathscr{P}(St = 1.02, M_{\text{tip}})$ spans a frequency range from 425 to 850 Hz when measurements were obtained at 11 equally spaced speeds between 2500 and 5000 rev/min. The values of $n_j(St)$ were determined using an ordinary least-squares fit, as well as a robust linear fit method, as described by Huber [23]. The robust fit was implemented using the `robustfit()` command in Matlab, which uses an iterative weighted adaptation of the least-squares method that reduces the influence of outliers on the linear fit. In a small number of cases, less than 1% for the present data set, the robust fit fails to converge, and an ordinary least-squares fit is used for these values of St.

Step 3: An improved estimate for $\log \mathscr{F}(St, M_{\text{tip}})$, denoted $\log \mathscr{F}'_j(St, M_{\text{tip}})$, is obtained using Eq. (24), along with $n_j(St)$ and $\log \mathscr{F}_{0,j}(St)$ from Step 2. This step can be expressed as

$$\log \mathscr{F}'_j(St, M_{\text{tip}}) = \log \mathscr{F}_{0,j}(St) + n_j(St) \log M_{\text{tip}}. \tag{25}$$

This new estimate of the source spectra is essentially a smoothed version based on the linear fit, and most of the transfer function effects should have been removed.

Step 4: An estimate for χ can now be found for each rotor speed using,

$$\log |\chi_{j+1}(f, M_{\text{tip}})|^2 = \log \mathscr{P}(f, M_{\text{tip}}) - \log \mathscr{F}'_j(f, M_{\text{tip}}) - \log k^2 - \log |g_{\text{fs}}|^2 - \log \cos^2 \theta, \tag{26}$$

as found in Eq. (21). The dimensionless source spectra $\mathscr{F}'_j(St, M_{\text{tip}})$ were used to obtain $\mathscr{F}'_j(f, M_{\text{tip}})$, and interpolation was again required to obtain data at the same points in f as the original measured sound spectra for use in Eq. (26). The transfer function effects can now be quantified as $\overline{\log |\chi_{j+1}(He)|^2}$, where the overbar denotes average over rotor speeds M_{tip}.

Step 5: The function $\overline{\log |\chi_{j+1}(He)|^2}$ calculated in the previous step can be used in place of $\log |\chi_j(He)|^2$ to iterate from Step 1.

Iterating between one and three times was found to provide a balance between a converged solution and a useful frequency range in the result. The example data from the ducted rotor in Fig. 5 are shown in Fig. 6 after one iteration. This indicates the transfer function features have been largely captured in $\chi(He)$, and the linear scaling is seen to be significantly improved.

4.2. Error analysis of the algorithm

A set of defined input functions was constructed in order to evaluate the effectiveness of the algorithm. The set consisted of a function for $\chi(He)$, a function for $\mathscr{F}_0(St)$ and a scaling $n(St)$. Spectral functions $\mathscr{P}(f, M_{\text{tip}})$ were created using Eq. (21) and used as input into the algorithm. The resulting function for $\chi(He)$ could then

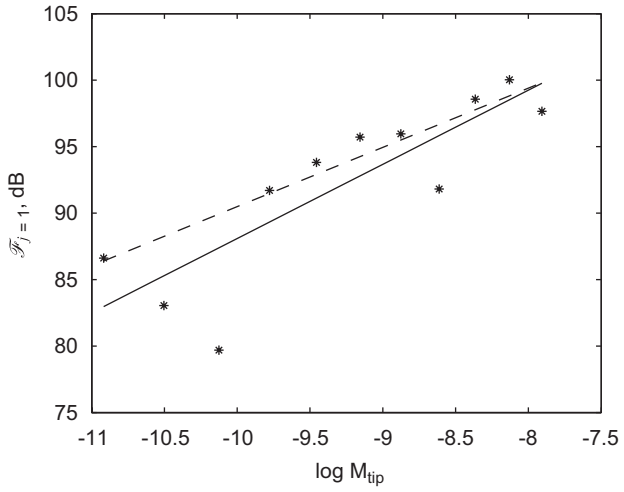

Fig. 5. Experimental data showing linear fit to $\log \mathscr{F}_{j=1}(St)$. '*': estimated sound source $\log \mathscr{F}_j(St = 1.02)$; '—': robust fit; '- - -': least-squares fit.

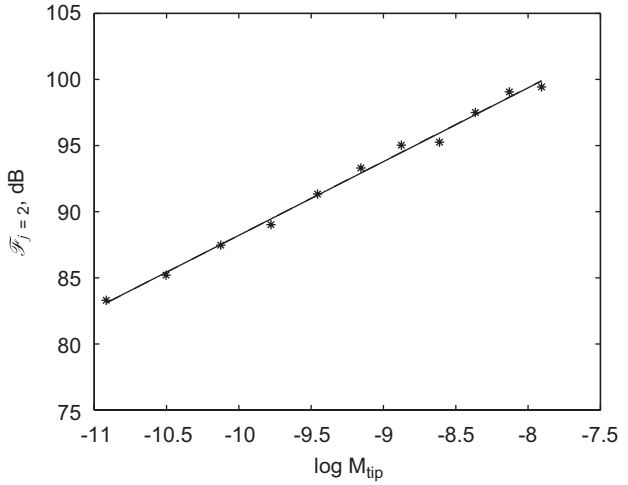

Fig. 6. Experimental data showing sound source linear scaling after one iteration of the algorithm. Transfer function effects have been largely removed. '*': estimated sound source $\log \mathscr{F}_{j=2}(St = 1.02)$; '—': robust fit; '- - -': least-squares fit.

be compared to the input, and an error computed by comparing the calculated transfer function ($\chi_C(He)$) to the actual transfer function ($\chi_A(He)$) as

$$\text{Error} = \sqrt{\frac{\int[\log|\chi_C(He)|^2 - \log|\chi_A(He)|^2]^2 \,\mathrm{d}He}{\int[\log|\chi_A(He)|^2]^2 \,\mathrm{d}He}}. \tag{27}$$

The transfer function $\log|\chi_A(He)|^2$ used for the defined input function set was a gaussian curve with a parameterized frequency width Δ_f and center frequency f_c given as

$$\log|\chi_A(He)|^2 = \mathrm{e}^{-10(f-f_c)^2/\Delta_f^2}. \tag{28}$$

This function is shown in Fig. 7. The feature shape can be considered a worst case, since the values were only positive and only induced outliers on one side of the correct linear slope in the $\log \mathscr{F}(St, M_{\text{tip}})$ vs. $\log M_{\text{tip}}$. A simple curve for the source spectra was used, $\log \mathscr{F}_0 = 30\cos(St/25) + 5\cos(2\pi St - \pi)\mathrm{e}^{-St}$. Other functional forms of the acoustic source were used, and the results indicate that the function χ did not depend on F_0. A scaling of $n = const$ was used for these results, although identical results were obtained when $n(St)$ was used. The experimental rotor tip speeds were used for M_{tip}.

A series of transfer functions were tested over a range of f_c and Δ_f and the error was computed. It was found that the error could be described by the functional relationship

$$\text{Error} = \text{function}\left(\frac{\Delta_f}{f_c}, \text{SR}\right), \tag{29}$$

where SR is the ratio of the maximum rotor speed to the minimum rotor speed. Specifically, the error curves at each SR collapsed when plotted against the *feature size ratio*, Δ_f/f_c. This is explicable because the range of f spanned at fixed St is a linear function of St. In this experiment, at $St = 1$ the 11 speeds span 416–833 Hz while at $St = 10$ the range is between 4160 and 8330 Hz. Lower St values result in frequency ranges that are smaller, such that if the transfer function changes only slightly across the frequency range it cannot be well resolved. The apparent size of a feature therefore depends on its center frequency 'location,' f_c, as well as its frequency 'width,' Δ_f. Note that this result is consistent with the previously mentioned limits on separating Eq. (18). Specifically, absolute magnitudes and linear trends in the transfer function cannot be described by finite values of Δ_f/f_c and thus cannot be determined.

The successful identification of transfer function features is also dependent on the speed ratio used during measurement. A small speed ratio results in points that are close together in f at constant St and only transfer function features that cause changes in that range of frequency can be identified. A larger speed ratio allows

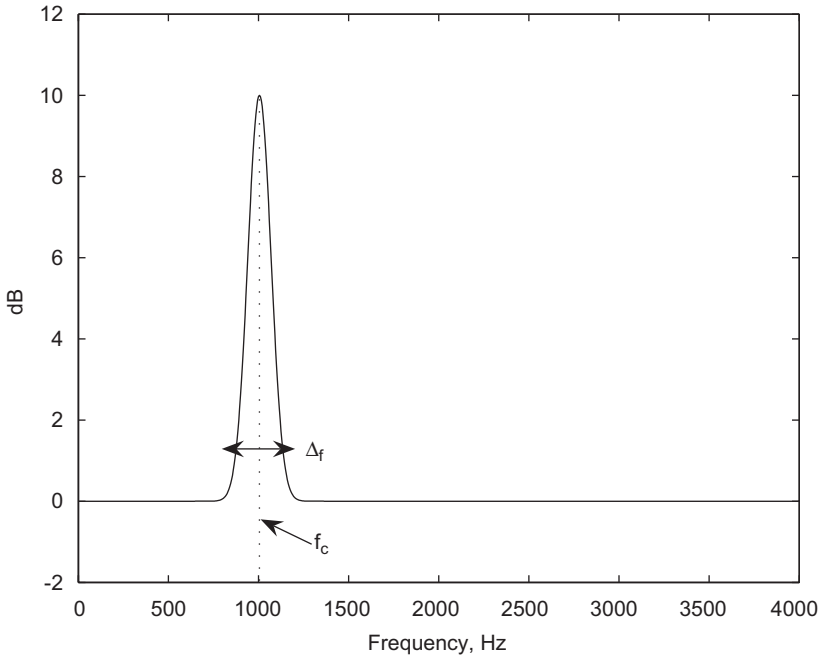

Fig. 7. Example simulated transfer function.

larger features to be identified. Minimum and maximum rotor speeds are limited by the experimental apparatus. Conversely, the limitation on using larger speed ratios is important when considering the scaling the spectra between *St* and *He*, as previously discussed. This restricts the number of iterations that can be performed, although adequate results can typically be obtained with only one or two iterations.

The error functions defined by Eq. (29) are shown in Fig. 8. As shown, for the set of defined input function tests using SR $=$ 2 and a feature of size 0.1 an error of 0.004 was calculated after one iteration and 0.0008 after two iterations. A larger feature with size of 0.2 resulted in an error value of 0.05 after one iteration and 0.03 after three iterations. Small features are well resolved under all speed ratios while larger features are poorly resolved. A higher speed ratio leads to lower error, especially for larger feature size ratios.

4.3. Results using experimental data

An effective test of the algorithm utilized data acquired from the ducted rotor experiment using the same duct geometry with a variety of rotor sound sources. Manipulating the rotor flow rate provided a method for varying the sound produced by the rotor without introducing additional sound sources into the system. Ingested turbulence, for example, could also have been varied, but turbulence generators may be a significant source of sound. The rotor flow coefficient ϕ was varied between rotor stall and zero pressure rise, as discussed in Section 3. The spectra for $\Omega = 5000\,\mathrm{rev/min}$ are shown in Fig. 9 at four flow coefficients. Substantial changes in the sound produced by the system can be observed, indicating that the source spectra was a strong function of ϕ.

The function $\chi(He)$ was calculated as specified in Section 4 using microphone measurements acquired at the four flow coefficients. These results are shown in Fig. 10 using two iterations of the algorithm. The frequency axis was normalized by the first organ pipe frequency based on duct length L calculated as

$$f_0 = \frac{c}{2(L + 0.6133D)}, \tag{30}$$

using the end correction as calculated by Levine and Schwinger [24]. The harmonics of predicted organ pipe modes are seen to correlate with peaks in the resultant transfer function. It is also clear

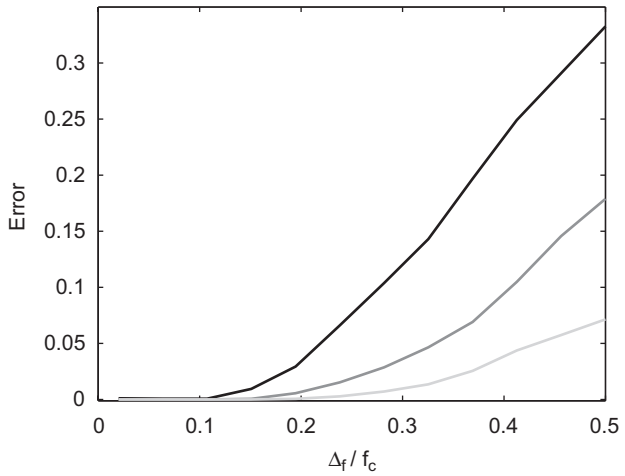

Fig. 8. Error defined by Eq. (27) for different values of feature size ratio and speed ratio after three iterations. '■': SR = 2; '■': SR = 3; '■': SR = 5.

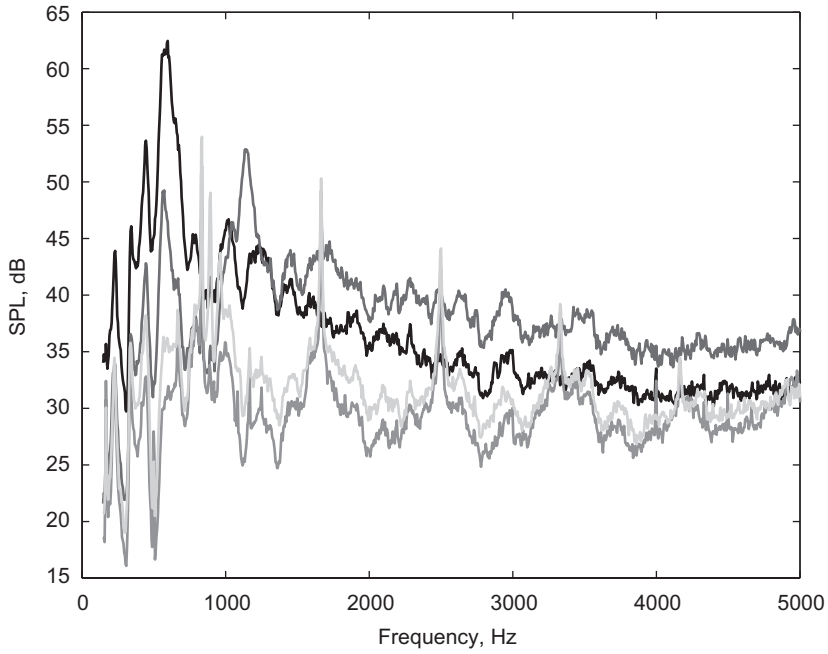

Fig. 9. Measured sound under different flow coefficients at 5000 rev/min. '■': $\phi = 0.17$; '■': $\phi = 0.22$; '■': $\phi = 0.30$; '■': $\phi = 0.42$.

that the function $\chi(He)$ determined by the algorithm is essentially independent of the acoustic source. The standard deviation between the four curves at each frequency was calculated, and a mean value of 0.29 dB was found.

Significant deviations are noted at only two frequencies, $f/f_0 \approx 1$ and $f/f_0 \approx 8$. At the lower frequency, the deviant χ values result from the lowest flow coefficient, $\phi = 0.17$. The rotor is stalled at this condition and the reduced magnitude was likely a result of changes in the coupling between the dipole source distribution and the duct plane waves. The deviant χ values at $f/f_0 \approx 8$ occurred at the highest flow coefficient, $\phi = 0.42$. At this condition the blades are completely unloaded and again, a change in the coupling between the blade dipoles and higher order duct modes could explain the variation in χ.

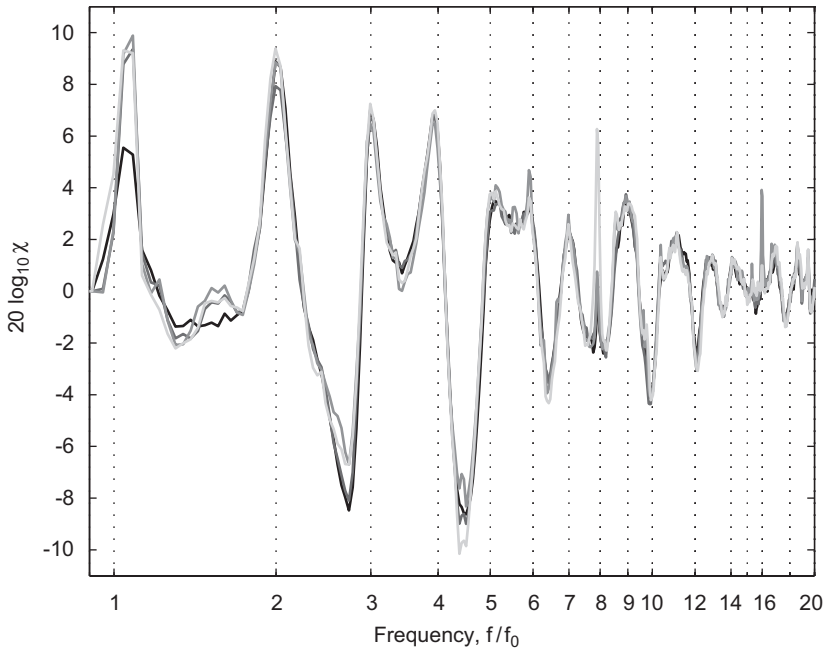

Fig. 10. Calculated functions $\chi(He)$ for $\phi = 0.17, 0.22, 0.30$ and 0.42 between 216 and 4791 Hz, normalized by the first organ pipe mode. Note that the first organ pipe mode $(f/f_0) = 1$ is at 112 Hz, which is at the lower limit of the usable frequency range of the anechoic facility. '■': $\phi = 0.17$; '■': $\phi = 0.22$; '■': $\phi = 0.30$; '■': $\phi = 0.42$.

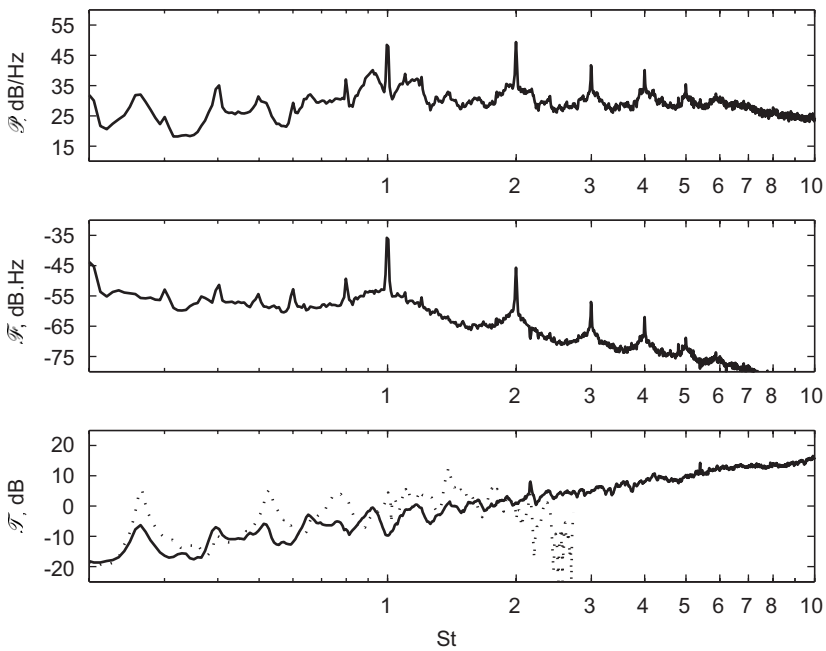

Fig. 11. Example sound spectra and decomposition results from algorithm showing sound pressure $\mathscr{P}$, unsteady force $\mathscr{F}$ and transfer function $\mathscr{T}$. The duct was configured with a length of 1.32 m. Operating conditions were $\phi = 0.30$, $\Omega = 5000$ rev/min. Measured sound was referenced to 20 μPa, unsteady force was referenced to 1 N and the dipole transfer function was referenced to $1/m^2$. '—': calculated results; '...': axial dipole transfer function obtained from reciprocity.

The final step in the analysis was to reconstruct the transfer function $\mathscr{T}(He)$ from the determined $\chi(He)$ function using Eq. (17). The sound source function $\mathscr{F}$ could be found using $\mathscr{T}$ and the measured sound spectra $\mathscr{P}$, as found in Eq. (18). An example of these three functions is shown in Fig. 11. As an independent validation of Eq. (17) and its assumptions, a reciprocal technique was used to obtain the dipole transfer function. Specifically, a miniature intensity probe was constructed, calibrated and placed in the duct at the axial position of the rotor with the blades removed. The dipole transfer function ($\nabla_0 g$) was then determined using the method of Fahy [25].

The transfer function determined using reciprocity is shown in Fig. 11 as a dotted line. The absolute magnitude and trend of the two curves support the present interpretation of Eq. (17) for $St<2$, corresponding to around 1700 Hz. Note that the features determined from reciprocity are greater in magnitude by up to 15 dB compared to the rotor transfer function $\mathscr{T}$ at integer multiples of f_0. This result is likely due to the absence of the blades during the reciprocity experiment. That is, the rotor would cause an effective impedance change in the duct which would reduce the organ pipe resonances. In addition, the true spatial distribution of the sources (axially and radially) that occurs in the rotor would lead to reduced resonant response.

5. Conclusions

A technique for processing aeroacoustic measurements was developed and evaluated. Using this algorithm the acoustic transfer function $\mathscr{T}$ could be determined. This will allow for the study of the sound source spectra $\mathscr{F}$ separate from acoustic transfer function effects. The method utilized the two frequency scales that are inherent in many applications to determine the functional form of a net equivalent source and a net acoustic transfer function from radiated sound spectra at various fan speeds. This was implemented as a computer algorithm, and evaluated with mathematically defined input functions, as well as experimental results from a low-speed ducted rotor.

The following conclusions were drawn from the study. First, any separation of net sources and net transfer function requires some form of assumption about either the source or the transfer function spectra. In the present algorithm, the acoustic source was assumed to increase with rotor speed to an unknown power. It was found that this assumption allowed for a unique determination of $\chi(He)$, which contained the narrow band spectral features of the acoustic transfer function $\mathscr{T}$. Second , the ability of the algorithm to determine spectral features of the net transfer function was quantified. Specifically, features whose width to center frequency ratio $\Delta_f/f_c<0.1$ were found to be correctly resolved with an error of less than 1% for a speed ratio of 2. This result was found to be independent of the spectral character of the acoustic source. Third, the algorithm was applied to a ducted rotor model operating under a range of flow coefficients. Transfer functions were calculated for each of these source conditions and were found to closely agree, with a standard deviation of 0.29 dB. The method effectively determines transfer function features from measured sound in a system where a net dipole source term is an appropriate approximation. Fourth, the spectral character of the ducted rotor transfer function was found to have peaks of magnitude up to ± 10 dB at integer multiples of the first duct organ pipe mode, in addition to other features. Finally, the magnitude and large-scale trend of the transfer function can be determined when a distribution of axially oriented dipoles is an appropriate approximation for the sound source. The magnitude and large-scale trends were verified using an independent reciprocity measurement of the transfer function.

References

[1] W.K. Blake, *Mechanics of Flow-induced Sound and Vibration (two volumes)*, Academic Press Inc., New York, 1986.
[2] M.E. Goldstein, *Aeroacoustics*, McGraw-Hill, New York, 1976.
[3] C.L. Morfey, Rotating blades and aerodynamic sound, *Journal of Sound and Vibration* 28 (3) (1973) 587–617.
[4] S.E. Wright, The acoustic spectrum of axial flow machines, *Journal of Sound and Vibration* 45 (2) (1976) 165–223.
[5] D.L. Huff, Fan noise prediction: status and needs, NASA/TM–97-206533, 1997.
[6] N. Moissev, B. Lakshminarayana, D.E. Thompson, Noise due to interaction of boundary-layer turbulence with a compressor rotor, *Journal of Aircraft* 15 (1) (1978) 53–61.
[7] R. Dunne, M.S. Howe, Wall-bounded blade-tip vortex interaction noise, *Journal of Sound and Vibration* 202 (5) (1997) 605–618.

[8] C. Lee, M.K. Chung, Y.H. Kim, A prediction model for the vortex shedding noise from the wake of an airfoil or axial flow fan blades, *Journal of Sound and Vibration* 164 (2) (1993) 327–336.
[9] H.M. Atassi, J. Fang, S. Patrick, Direct calculation of sound radiated from bodies in nonuniform flows, *Journal of Fluids Engineering* 115 (1993) 573–579.
[10] H. Kobayashi, Three dimensional effects on pure tone fan noise due to inflow distortion, *AIAA 11th Fluid and Plasma Dynamics Conference*, Seattle, Washington, July 10–12, 1978.
[11] P.E. Doak, Excitation transmission and radiation of sound from source distributions in hard-walled ducts of finite length (i): the effects of duct cross-section geometry and source distribution space–time pattern, *Journal of Sound and Vibration* 31 (1) (1973) 1–72.
[12] P.E. Doak, Excitation, transmission and radiation of sound from source distributions in hard-walled ducts of finite length (ii): the effects of duct length, *Journal of Sound and Vibration* 31 (2) (1973) 137–174.
[13] A.D. Pierce, *Acoustics: An introduction to its Physical Principles and Applications*, McGraw-Hill, New York, 1981.
[14] J. Weidemann, Analysis of the relations between acoustic and aerodynamic parameters for a series of dimensionally similar centrifugal fan rotors, NASA Technical Translation NASA TT F-13, 798, 1971.
[15] W. Neise, Application of similarity laws to the blade passage sound of centrifugal fans, *Journal of Sound and Vibration* 43 (1) (1975) 61–75.
[16] P. Bent, D. McLaughlin, Enhancements to noise source measurement techniques for turbomachinery, *15th AIAA Aeroacoustics Conference*, Long Beach, California, October 25–27, 1993.
[17] L. Mongeau, D.E. Thompson, D.K. McLaughlin, A method for characterizing aerodynamic sound sources in turbomachines, *Journal of Sound and Vibration* 181 (3) (1995) 369–389.
[18] Z. Zhang, L. Mongeau, S.H. Frankel, Broadband sound generation by confined turbulent jets, *Journal of the Acoustical Society of America* 112 (2) (2002) 677–689.
[19] P.M. Morse, K.U. Ingard, *Theoretical Acoustics*, Princeton University Press, Princeton, NJ, 1968.
[20] W. Neise, B. Barsikow, Acoustic similarity laws for fans, *Journal of Engineering for Industry* 104 (1982) 162–168.
[21] D.A. Quinlan, M.H. Krane, Aeroacoustic source identification using frequency dependent velocity scaling, *Second AIAA and CEAS Aeroacoustics Conference*, State College, Pennsylvania, May 6–8, 1996.
[22] M. Sevik, Sound radiation from a subsonic rotor subjected to turbulence, *NASA SP* 304 (11) (1974) 493–511.
[23] P.J. Huber, *Robust Statistics*, Wiley, New York, 1981.
[24] H. Levine, J. Schwinger, On the radiation of sound from an unflanged circular pipe, *Physical Review* 73 (4) (1948) 383–406.
[25] F. Fahy, Some applications of the reciprocity principle in experimental vibroacoustics, *Acoustical Physics* 42 (3) (2003) 217–229.